INTERNATIONAL JOURNAL OF REFRIGERATION 60 (2015) 278–288

Available online at www.sciencedirect.com

ScienceDirect

journal homepage: www.elsevier.com/locate/ijrefrig

Electrochemical compressor driven metal hydride heat pump

Ye Tao [a], *Hoseong Lee* [a], *Yunho Hwang* [a,*], *Reinhard Radermacher* [a], *Chunsheng Wang* [b]

[a] *Center for Environmental Energy Engineering, University of Maryland, 4164 Glenn L. Martin Hall Bldg., College Park, MD 20742, USA*

[b] *Department of Chemical and Biomolecular Engineering, 1223A Chemical & Nuclear Engineering Bldg., University of Maryland, College Park, MD 20742, USA*

ARTICLE INFO

Article history:
Received 21 May 2015
Received in revised form 30 July 2015
Accepted 25 August 2015
Available online 28 August 2015

Keywords:
Electrochemical compressor
Metal hydride
Heat pump
Proton exchange membrane

ABSTRACT

In this study, a new metal hydride heat pump system driven by an electrochemical compressor was proposed. The system uses the electrochemical compressor to generate absorption heating and desorption cooling in two identical $LaNi_5$ reactors operating at different pressure levels. A thermodynamic model was developed to predict the system performance in terms of various parameters. Modeling shows EC compression efficiency has a great impact on system performance. The system is suitable for cooling application less than 200 W where mechanical compressors are the most inefficient. The high compression efficiency of electrochemical compressor could potentially make the cooling system more competitive than existing metal hydride heat pump systems.

Pompe à chaleur en hydrure métallique entrainée par un compresseur électrochimique

Mots-clés : Compresseur électrochimique ; Hydrure métallique ; Pompe à chaleur ; Membrane d'échange de proton

1. Introduction

In the United States, heating ventilation and air conditioning (HVAC) system accounts for 41% of commercial building energy consumption and 36% of residential building energy consumption (Goetzler et al., 2014). Most of the energy consumed by the HVAC system in residential and commercial buildings is used for space heating and cooling, which is mostly based on the vapor compression cycle. Conventional vapor compression cycles use refrigerants such as R-134a and R-410A that have high global warming potential. Therefore,

* *Corresponding author.* Center for Environmental Energy Engineering, University of Maryland, 4164 Glenn L. Martin Hall Bldg., College Park, MD 20742, USA. Tel.: +1 301 405 5286; Fax: (301) 405-2025.
E-mail address: yhhwang@umd.edu (Y. Hwang).

http://dx.doi.org/10.1016/j.ijrefrig.2015.08.018

Nomenclatures

Symbols

A	activated cell area [cm^2]
F	Faraday's constant [$c \cdot mol^{-1}$]
ΔH	enthalpy change of formation [$kJ \cdot mol^{-1}$]
I_d	current density [$A \cdot cm^{-2}$]
I	current [A]
N	number of electrochemical compressors connected in parallel
P	pressure [bar]
Q	capacity [W]
R	gas constant [$J \cdot mol^{-1} \cdot K^{-1}$]
R_i	internal resistance [$\Omega \cdot cm^2$]
ΔS	entropy change of formation [$kJ \cdot mol^{-1} \cdot K^{-1}$]
T	temperature [°C]
U_{ac}	cathode and anode polarization [V]
U_{Nernst}	Nernst potential [V]
U_{ohm}	ohmic loss [V]
W_{EC}	power consumption [W]

Subscript: acronyms

a	absorption
c	cooling
COP	coefficient of performance
d	desorption
dis	discharge
EC	electrochemical compressor
eff	effectiveness
eq	equilibrium
h	heating
HVAC	heating ventilation and air conditioning
hyst	hysteresis
i	internal
in	indoor
m	midpoint of plateau
MEA	membrane electrolyte assembly
MH	metal hydride
o	reference
out	outdoor
R	reactor
s	surface
suc	suction

solid state cooling technologies have been developed to address the global warming challenges and enhance the efficiency. Metal hydride (MH) cooling and heating technologies are developed with metals or alloys, which can absorb hydrogen reversibly to form MHs. The reaction can be described as eq. (1) (Hirscher, 2010; Sandrock, 1999).

$$M + \frac{x}{2}H_2 \leftrightarrow MH_x + Q \quad (1)$$

where Q is the heat of reaction of hydride formation.

Absorption reaction is exothermic, while desorption reaction is endothermic, based on eq. (1). A metal can absorb or desorb hydrogen at given temperature depending on its phase equilibrium plateau pressure (P_m). The absorption process is shown in Fig. 1. Initially, the metal can dissolve some hydrogen atoms into its lattice to form a solid solution (α phase). When either the hydrogen concentration or the pressure increases further at a given temperature, a MH phase (β phase) starts to form. Starting at that point, a plateau is observed where both α and β phases coexist (Hirscher, 2010). The plateau is similar to the latent heat of a pure substance, such as the latent heat of evaporating water. The Van't Hoff equation below (eq. (2)) describes the midpoint plateau pressure in relation with temperature at given enthalpy of formation and entropy of formation (Hirscher, 2010; Sandrock, 1999).

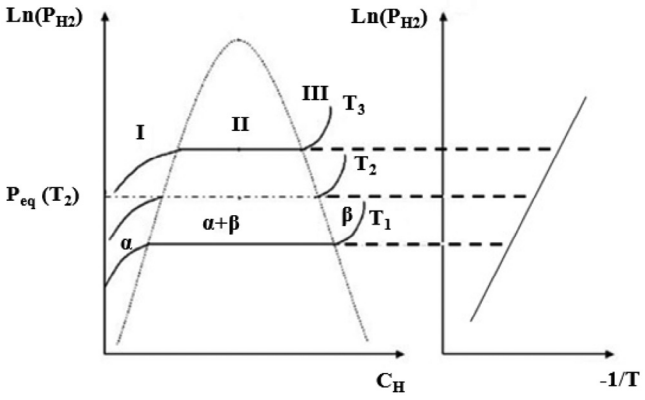

Fig. 1 – Pressure–composition isotherms of MH.

$$\ln\left(\frac{P_m}{P_0}\right) = \frac{\Delta H}{RT} - \frac{\Delta S}{R} \quad (2)$$

where P_0 is the reference pressure of 1 bar, and R is the gas constant. Under a given temperature, the metal absorbs hydrogen when the pressure is above the plateau pressure, while below the plateau pressure, the hydride (β phase) is unstable and releases hydrogen.

Nafion is widely used in fuel cells as the proton exchange membrane (Barbir, 2005; Benziger et al., 2011). EC working mechanism is shown in Fig. 2. With the help of a catalyst such as platinum, hydrogen decomposes to protons and electrons on one side of the membrane (anode) and then protons travel across the membrane. Whereas electrons take a different route, driven by an external voltage to the other side (cathode) where they recombine with protons to regenerate hydrogen. As long as the driving force (voltage) is constant, hydrogen transfer across the membrane can happen at a constant rate, which can be calculated from Faraday's Law (Rohland et al., 1998) in eq. (3).

$$\frac{dn}{dt} = \frac{I}{2F} \quad (3)$$

where dn/dt is the hydrogen flowrate across the membrane, I is the current generated by the voltage supply, F is Faraday's constant. If hydrogen is transferred to the cathode with a constant volume that is less than the anode, the pressure on the cathode increases and an electrochemical compressor is therefore developed. Since clean hydrogen is re-produced at the

Table 1 – Electrochemical compressor compression limit.

Group	EC compression pressure achieved (bar)	MEA	Activated area (cm^2)
Rohland et al. (1998)	43	ETEK MEA Nafion 117	100
Strobel et al. (2002)	54	ZSW MEA Nafion 115	100
Grigoriev et al. (2011)	130	Nafion 117	25
Lipp (2012)	827	N/A	200
Bouwman (2014)	1000	N/A	N/A

cathode through chemical reactions, there is very little contamination (Rohland et al., 1998; Strobel et al., 2002). Several studies have been conducted by different groups to investigate the EC performance (Gardner and Ternan, 2007; Grigoriev et al., 2011; Onda et al., 2007; Rohland et al., 1998; Sedlak et al., 1981; Strobel et al., 2002). According to the research done previously, the pressure limit of hydrogen reached by the EC from atmospheric pressure can vary from 20 bar to 1000 bar (Bouwman, 2014; Grigoriev et al., 2011; Lipp, 2012; Lipp and Patel, 2011; Rohland et al., 1998; Strobel et al., 2002). In order to achieve very high pressure, multiple stacks of ECs are required, and membranes need to be backed up with supporting material. The efficiency of EC can be around 90% at small hydrogen flowrates (Bouwman, 2014; Lipp, 2012; Lipp and Patel, 2011). The comparison of different selected ECs developed is listed in Table 1.

Because of the exothermic and endothermic behaviors of absorption and desorption processes, MH has been previously studied for heat pumps. The heat pump systems have been reviewed by different authors (Muthukumar and Groll, 2010; Takeda et al., 2009). There are mainly two ways of using MH as heat pumps: heat driven MH heat pump, and compressor driven MH heat pump (Muthukumar and Groll, 2010; Takeda et al., 2009). The heat driven MH heat pump is based on transferring hydrogen between two or more reactors, exploiting the different absorption and desorption pressures and temperatures of each reactor to generate heating or cooling (Muthukumar and Groll, 2010). As shown in Fig. 3, low temperature MH reactor A and high temperature MH reactor B are connected. Each reactor contains a different MH material. During the operation, MH reactor A releases hydrogen by taking up waste heat at low temperature. Hydrogen released flows to the other reactor which absorbs hydrogen at high temperature to generate useful space heating. The cooling process takes place when the high temperature MH reactor B is cooled by rejecting heat to the air and absorbs hydrogen, which reduces the hydrogen pressure of the system and causes low temperature MH reactor A to desorb hydrogen and generates useful space cooling. This type of the MH heat pump usually has COP less than 1 (Zhong and Glanville, 2014). The compressor driven MH heat pump usually uses two identical MH reactors (Muthukumar and Groll, 2010; Takeda et al., 2009). A mechanical compressor reduces the pressure of the desorption reactor and increases the pressure of absorption reactor (Fig. 4) (Kim et al., 1997). Thus one reactor desorbs hydrogen and generates cooling at low pressure and temperature, while the other reactor absorbs hydrogen and generates heating at high pressure and temperature. The compressor driven MH heat pump is studied by various groups using a mechanical compressor to maintain the pressure difference by driving hydrogen from one reactor to the other (Kim et al., 1997; Magnetto et al., 2006; Mazumdar et al., 2004; Park et al., 2001, 2002). Table 2 lists previous mechanical compressor driven MH heat pump developed by different groups. Kim et al. (1997) conducted steady state simulation and calculated the COP of LaNi5 system to be 4.3 for a 3.5 kW system with cooling temperature at 8 °C and heating temperature at 46 °C, however, they did not con-

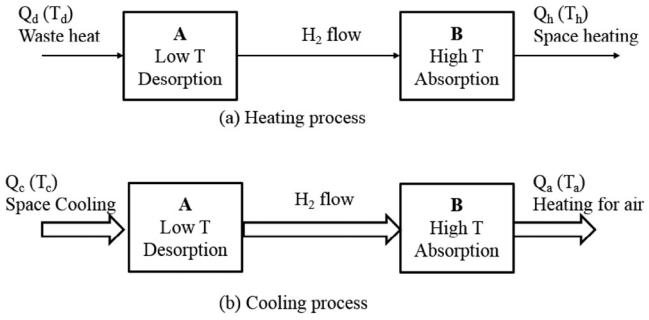

Fig. 3 – Heat driven MH heat pump, using the difference of absorption and desorption pressure of different MH materials.

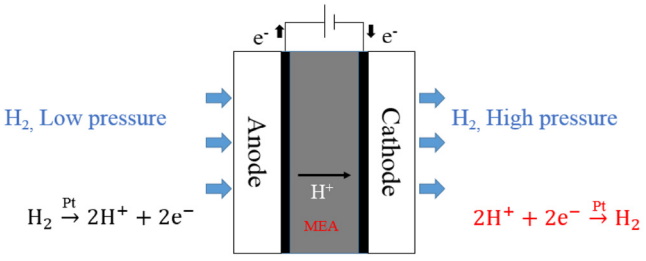

Fig. 2 – Working principle of EC.

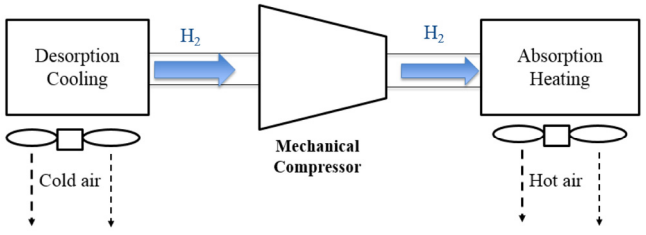

Fig. 4 – Mechanical compressor driven MH heat pump.

Table 2 – Compressor driven MH heat pump.

Group	Approach	COP	Temperature lift (°C)	Capacity (kW)	MH type
Kim et al. (1997)	Steady state simulation	4.3	8–46	3.5	LaNi5
Park et al. (2002)	Experiment	1.8	6–32	1.4	$Zr_{0.9}Ti_{0.1}Cr_{0.55}Fe_{1.45}$
Mazumdar et al. (2004)	Transient simulation	2.5	22–32	1	$Zr_{0.9}Ti_{0.1}Cr_{0.55}Fe_{1.45}$
Magnetto et al. (2006)	Experiment	2.6	20–45	2	Mm based alloy

sider the hysteresis of the MH material, pressure drop during suction and discharge of hydrogen, and heat exchanger effectiveness, so their modeling results might be a bit optimistic. Park et al. (2002) conducted the experiment on $Zr_{0.9}Ti_{0.1}Cr_{0.55}Fe_{1.45}$ and measured the COP to be 1.8 for a 1.4 kW system with cooling temperature at 6 °C and heating temperature at 32 °C. Mazumdar et al. (2004) conducted the transient simulation using $Zr_{0.9}Ti_{0.1}Cr_{0.55}Fe_{1.45}$, taking into account the heat transfer and calculated the COP to be 2.5 with cooling temperature at 22 °C and heating temperature of 32 °C for a 1 kW system. Magnetto et al. (2006) developed a prototype of Mm based alloy that shows COP of 2.6 for a 2 kW system with cooling temperature at 20 °C and heating temperature at 45 °C.

The existing MH heat pump technologies have their limitations. The heat driven MH heat pump has a low COP, while the mechanical compressor efficiency limits the mechanical compressor driven MH heat pump performance. Currently, small hydrogen compressors required for small compressor driven metal hydride cooling systems with less than 200 W of cooling capacity have around 65% isentropic efficiency. Moreover, the compressed hydrogen usually contains traces of lubrication oil that potentially reduce the MH absorption and desorption performance. In order to solve all above limitations, the EC driven MH heat pump was proposed in this paper, and its system performance was investigated.

2. Process description for EC driven MH heat pump

The MH heat pump system driven by the EC is similar to the previously developed mechanical compressor driven MH heat pump as two identical MH reactors, one for cooling and one for heating, are connected by the compressors in both systems. However, in the proposed MH heat pump system, the mechanical compressor is replaced by the EC. As shown in Fig. 5, the EC is placed in between two identical $LaNi_5$ MH reactors so that one side generates cooling at low pressure and the other side produces heating at high pressure. Hydrogen is desorbed from the MH reactor, where pressure is below the plateau pressure at low system pressure and temperature of heat source. Meanwhile, hydrogen is pumped to and absorbed in the MH reactor on the other side where the pressure is above the plateau pressure at high system pressure and temperature of heat sink. $LaNi_5$ was chosen for modeling, because it is the most commonly used MH for heat pump development as pointed out from the most recent review papers (Sandrock and Bowman, 2003; Zhong and Glanville, 2014). In addition, $LaNi_5$ and its AB_5 hydride family absorb and desorb hydrogen in room temperature at reasonable pressure range (100–400 kPa) with small hysteresis (Hirscher, 2010; Sandrock, 1999).

The uniqueness of choosing EC to be the compressor is that the anode and cathode of the EC are both identical, which makes it possible to switch hydrogen flow direction by switching the polarity of power supply. A continuously operating system of the EC heat pump with indoor and outdoor heat exchangers is therefore proposed. As it is shown in Fig. 6, initially, the reactor on the left (bed 1) is full of hydrogen and reactor on the right (bed 2) is empty of hydrogen. After the EC is turned on, hydrogen pressure is reduced in the left reactor as desorption occurs, so that temperature drops and cooling is generated at T_d (Fig. 6a). This cold reactor is in heat exchange with the indoor heat exchanger. As pressure increases on the right reactor (bed 2), absorption occurs so that temperature increases and heating is generated at T_a. This hot reactor is in heat exchange with the outdoor heat exchanger. When bed 1 is depleted and bed 2 is full, bed 1 (cold) is preheated and bed 2 (hot) is pre-cooled by air at room temperature (Fig. 6b). Finally, as shown in Fig. 6c, the polarity of power supply is switched, so that hydrogen flows from bed 2 to bed 1, bed 2 therefore generates cooling and bed 1 generates heating by switching the heat transfer fluid flow of corresponding indoor and outdoor heat exchangers. The cycle operation of MH is shown on the Van't Hoff chart (Fig. 7).

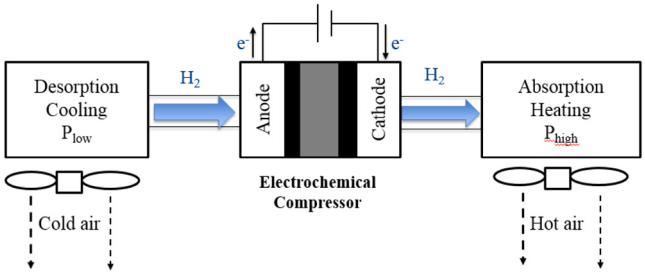

Fig. 5 – Design of EC driven MH heat pump.

3. Thermodynamic analysis of the system

For the analysis of MH heat pump with EC, the thermodynamic model was developed with following assumptions:

- The EC is the only power consumer in the system, power consumed by other parts such as pumps and fans of heat exchangers are neglected.
- Enthalpy of formation (ΔH) and entropy of formation (ΔS) of MH do not change with temperature.

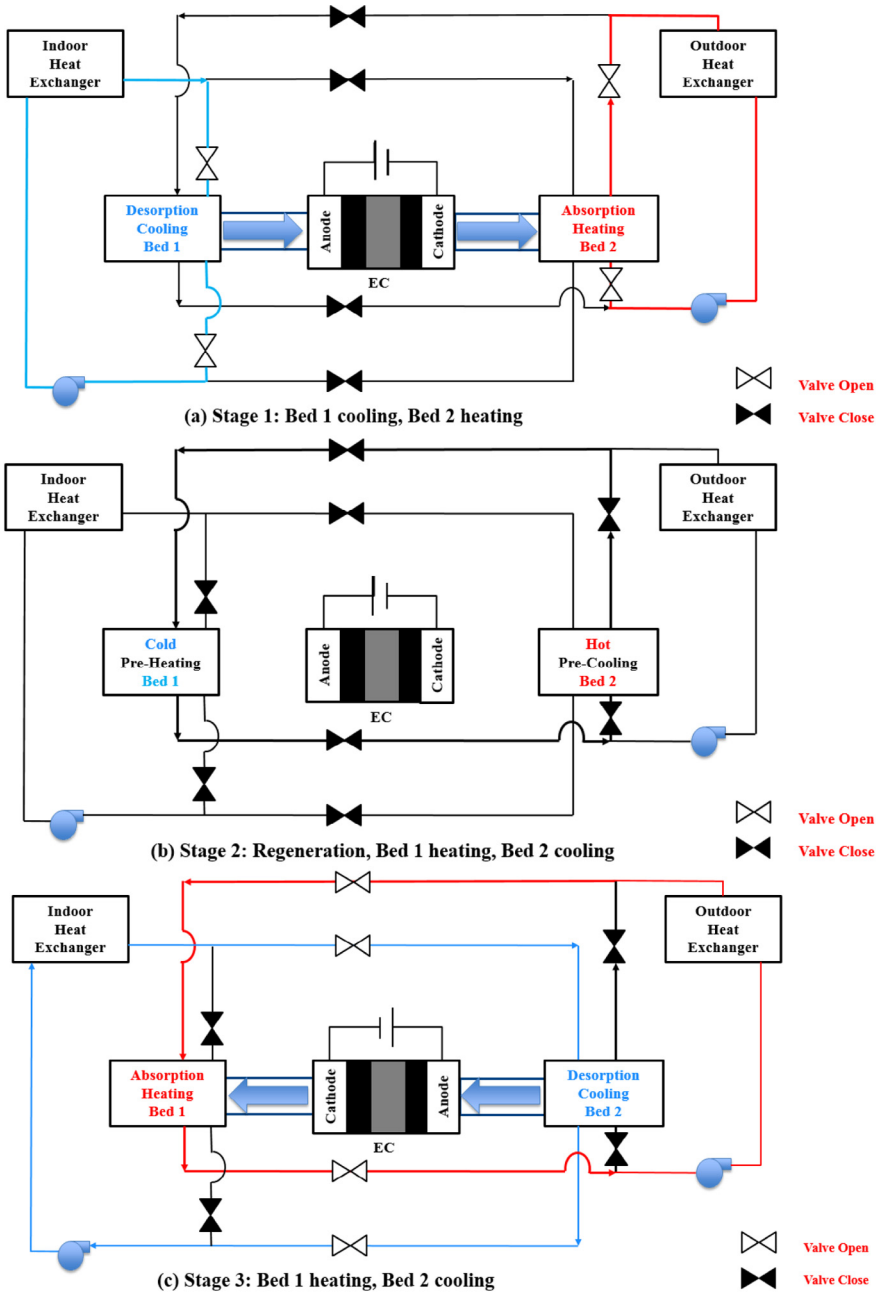

Fig. 6 – Schematic diagram of EC system; Stage 1: bed 1 cooling, bed 2 heating; Stage 2: regeneration, bed 1 heating, bed 2 cooling; Stage 3: bed 1 heating, bed 2 cooling.

- Metal hydride packing in the reactor is homogeneous, meaning there is no spatial distribution of temperature, and hydrogen concentration in the hydride packing is uniform.
- Modeling is based on system at steady state. Proton transfer across the membrane is only dependent on current density.
- Back diffusion of hydrogen across the membrane is not considered due to non-significant pressure gradient.
- Electronic resistance on current collectors is neglected because it is very small (Barbir, 2005). Therefore, total cell internal resistance only accounts for membrane ionic and contact resistance.

The relationship between the midpoint of plateau pressure and temperature can be expressed with Van't Hoff's equation (eq. (4)).

$$P_m = \exp\left(\frac{\Delta H}{RT} - \frac{\Delta S}{R}\right) \tag{4}$$

Desorption pressure is calculated by taking into account the plateau slope and hysteresis as shown in eqs. (5)–(7).

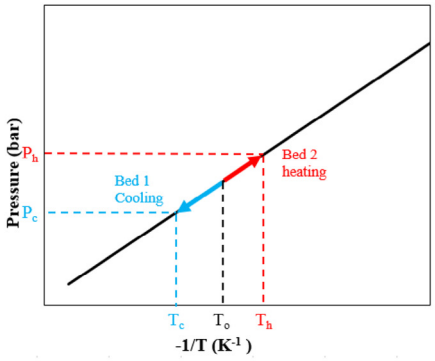

(a) Stage 1: Bed 1 cooling and Bed 2 heating

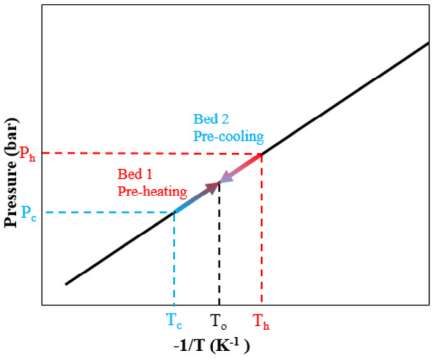

(b) Stage 2: Regeneration, Bed 1 pre-heating and Bed 2 pre-cooling

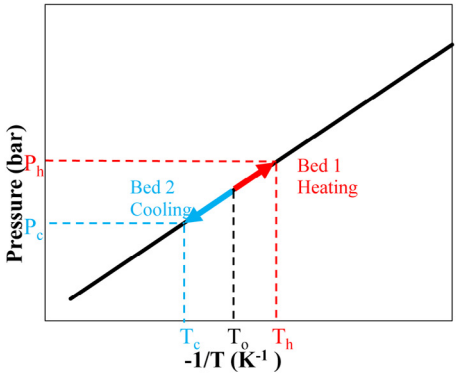

(c) Stage 3: Bed 1 heating, Bed 2 cooling

Fig. 7 – Heating and cooling cycles of $LaNi_5$.

$$\ln P_c = \frac{\Delta H}{RT} - \frac{\Delta S}{R} + f_s(C - C_{eq}) - \ln\left(\frac{P_a}{P_d}\right)_{T_c} \quad (5)$$

$$\ln P_h = \frac{\Delta H}{RT} - \frac{\Delta S}{R} + f_s(C - C_{eq}) + \ln\left(\frac{P_a}{P_d}\right)_{T_h} \quad (6)$$

$$f_s = \frac{\ln P - \ln P_{eq}}{C - C_{eq}} \quad (7)$$

where P_c and P_h are the pressures of desorption (cooling) and absorption (heating), f_s is the plateau slope factor and $C - C_{eq}$ is the change of hydrogen content in the alloy.

For characterization of the MH, the pressure at the midpoint of the plateau is taken without considering the plateau slope (Hirscher, 2010). $\ln(P_a/P_d)_T$ is the hysteresis factor at given temperature. Hysteresis is represented by the free energy difference (Hirscher, 2010) as in eq. (8).

$$\frac{\Delta G_{hyst}}{RT} = \ln\left(\frac{P_a}{P_d}\right)_T \quad (8)$$

where P_a and P_d are the absorption and desorption pressures at the given temperature.

The EC suction and discharge pressure are calculated in eqs. (9) and (10) based on absorption and desorption pressures plus the pressure drop between desorption reactor and EC inlet as well as absorption tank and EC outlet.

$$P_{suc} = P_c - \Delta P_{suc} \quad (9)$$

$$P_{dis} = P_h + \Delta P_{dis} \quad (10)$$

The MH desorption and absorption temperatures are calculated in eqs. (11) and (12) based on cooling and heating temperatures as well as the temperature differences for heat transfer between the reactors and surrounding.

$$T_d = T_c - \Delta T_d \quad (11)$$

$$T_a = T_h + \Delta T_a \quad (12)$$

The amount of MH required for the system is calculated in eq. (13) based on the cylindrical reactor volume.

$$m_{MH} = \pi r_1^2 * H_R * vr * \rho_{MH} \quad (13)$$

where r_1 is the reactor inner radius, H_R is the reactor length, vr stands for the percentage of reactor volume occupied by MH packing.

The metal hydride and metal hydride container must be sensibly cooled during refrigeration process, and sensibly heated during regeneration process, therefore, this parasitic loss needs to be considered. The entire cooling cycle includes desorption time, sensible cooling down time and regeneration time as in eq. (14).

$$t_{cycle} = t_d + t_{cd} + t_{rg} \quad (14)$$

Desorption time is calculated in eq. (15) from the amount of hydrogen stored in the MH packing, and the rate of hydrogen flowing out of container. The storage capacity of $LaNi_5$ is taken to be 1.5% by weight (Sandrock, 1999).

$$t_d = \frac{m_{MH} * 1.5\%}{\frac{dn}{dt} * 2} \quad (15)$$

The sensible cooling down time (t_{cd}) for MH packing and the reactor is found in eq. (16) based on the enthalpy of desorption and hydrogen flow rate.

$$t_{cd} = \frac{(C_{MH} * m_{MH} + C_R * m_R) * \Delta T_{cd}}{\Delta H_d * \frac{dn}{dt}} \quad (16)$$

where ΔT_{cd} stands for the cooling down temperature.

The regeneration time can be found in eq. (17) based on the convection heat transfer between the reactor and the ambient.

$$t_{rg} = \frac{(C_{MH} * m_{MH} + C_R * m_R) * \Delta T_{rg}}{h_x * A_R * \Delta T_{rg}} \quad (17)$$

where h_x stands for the cylinder convection heat transfer coefficient, it is calculated in eq. (18) based on the Zhukauskas relation for flow over cylindrical surface (Incropera and Dewitt, 2002). ΔT_{rg} stands for the temperature change due to regeneration. A_R stands for the surface area of the reactor.

$$h_x = Nu * \frac{k}{D} = \frac{k}{D} C Re^m Pr^n \left(\frac{Pr}{Pr_s}\right)^{\frac{1}{4}} \quad (18)$$

where Nu is the Nusselt number, D is the outer diameter of the reactor, k is the air thermal conductivity, Re is Reynold's number, Pr is the Prandtl number.

During the regeneration process, both hot and cold metal hydride reactors are either pre-cooled or pre-heated by air at room temperature until thermal equilibrium has been reached. Therefore, the cooling power is calculated in eq. (19) by taking the average of total cooling energy generated in terms of cooling cycle time.

$$\overline{Q_c} = \frac{\Delta H_d * \frac{dn}{dt} * t_d * hx_{eff}}{t_{cycle}} \quad (19)$$

where hx_{eff} is the heat exchanger effectiveness.

The heating power is calculated in the similar manner, as well as considering the time for heating up the metal hydride and the metal hydride container, and the regeneration time.

For modeling the EC, the total cell voltage of EC is expressed in eq. (20).

$$U = U_{Nernst} + U_{ohm} + U_{ac} \quad (20)$$

where U_{Nernst} stands for the Nernst potential, U_{ohm} is the ohmic loss of the cell due to total cell internal resistance, U_{ac} stands for the anode and cathode polarization. For EC, since there is no oxygen which reacts on the cathode side to produce water, the cathode and anode polarization are very small and can therefore be neglected (Onda et al., 2007; Strobel et al., 2002). Thus the above equation is reduced to eq. (21).

$$U = U_{Nernst} + U_{ohm} \quad (21)$$

U_{Nernst} can be calculated in eq. (22) from the Nernst equation.

$$U_{Nernst} = \frac{RT_{EC}}{2F} \ln\left(\frac{P_{dis}}{P_{suc}}\right) \quad (22)$$

U_{ohm} of a single EC satisfies Ohm's law (Barbir, 2005) as shown in eq. (23).

$$U_{ohm} = I_d * R_i = \frac{I}{N * A} * R_i \quad (23)$$

where I_d is the current density of a single EC, I is the total current generated by the power supply, N is the number of ECs connected in parallel, A is the active cell area. A typical value for R_i, depending on the thickness of Nafion membrane, is between 0.05 and 0.2 $\Omega \cdot cm^2$ (Barbir, 2005; Mehta and Cooper, 2002). The lower side value of 0.05 $\Omega \cdot cm^2$ is taken for Nafion 115 membrane with 125 μm thickness. The total power required for the EC is calculated in eq. (24) by multiplying the total cell voltage by the total current.

$$W_{EC} = (U_{ohm} + U_{Nernst}) * I \quad (24)$$

The electrochemical compression efficiency is the ratio between Nernst power (W_{Nernst}) and total power input required for the MEA (W_{EC}), based on the analogy of PEM fuel cell power efficiency (Barbir, 2005) as shown in eq. (25).

$$\bullet_{EC} = \frac{W_{Nernst}}{W_{EC}} \quad (25)$$

where the total power required for the EC is W_{EC}, which is the sum of U_{Nernst} and work generated by internal resistance. Therefore, η_{EC} can be calculated from eq. (26).

$$\eta_{EC} = \frac{U_{Nernst} * I}{(U_{ohm} + U_{Nernst}) * I} \quad (26)$$

which is further reduced to the ratio of Nernst potential and total cell voltage as in eq. (27):

$$\eta_{EC} = \frac{U_{Nernst}}{U_{Nernst} + U_{ohm}} = \frac{\frac{RT_{EC}}{2F} \ln\left(\frac{P_{dis}}{P_{suc}}\right)}{\frac{RT_{EC}}{2F} \ln\left(\frac{P_{dis}}{P_{suc}}\right) + I_d R_i} \quad (27)$$

The similar calculation for EC efficiency is also developed by Wong et al. (2004).

The EC power is calculated in eq. (28) based on the total amount of energy required divided by the cooling cycle time.

$$\overline{W_{EC}} = \frac{(U_{ohm} + U_{Nernst}) * I * t_d}{t_{cycle}} \quad (28)$$

The cooling COP of system can therefore be calculated as in eq. (29).

$$COP = \frac{\overline{Q_c}}{\overline{W_{EC}}} \quad (29)$$

4. Simulation results and discussion

The hydrogen flow rate across the membrane is only related to the current density for steady state analysis. Therefore, the current density can be treated in analogy to hydrogen flow rate across the membrane. Table 3 lists all the design parameters for the steady state simulation. The cross sectional area of 100 cm^2 was chosen for the EC based on the experimental work done by Rohland et al. (1998). The membrane resistance was

Table 3 – Fixed design parameters for steady state simulation.

Parameters	Symbol	Value	Units
Cross sectional area	A	100	cm^2
Membrane internal resistance	R_i	0.05	$\Omega \cdot cm^2$
Number of ECs in parallel	N	20	ea
Heat of formation	ΔH	30.8	$kJ \cdot mol^{-1}$
Entropy of formation	ΔS	0.108	$kJ \cdot mol^{-1} \cdot K^{-1}$
Membrane operating temperature	T_{EC}	343	K
Outdoor temperature	T_h	308	K
Room temperature	T_c	288	K

taken assuming thinner membrane is selected for the EC based on the available resistance values. The metal hydride enthalpy of formation and entropy of formation were both taken from existing measurement (Sandrock, 1999). The EC operating temperature was chosen according to Moton et al. (2014). The effects of current density, mass ratio between MH and reactor, suction and discharge pressure drop, desorption and absorption temperature drop were studied by keeping other parameters constant at 10 K for ΔT_d, 10 K for ΔT_a, 0.2 for $\Delta P_{dis}/P_{dis}$, 0.1 for $\Delta P_{suc}/P_{suc}$, 1.9 for R_m, 0.05 $A \cdot cm^{-2}$ for current density, 20 for number of ECs in parallel. Some parameters were selected based on research done by Bedback and Gopal (2004) on compressor driven metal hydride heat pump. Other physical properties for $LaNi_5$ MH and its reactor were taken from the study done by Hopkins and Kim (2010), and are listed in Table 4.

Fig. 8 shows the effects of current density on system performance at constant mass ratio between MH and reactor. The cooling power increases with current density because the hydrogen flow rate increases. Meanwhile, the COP decreases. This is due to the increased ohmic loss on the EC unit, and it continuously plays a role on decreasing the compression efficiency of EC, therefore decreases the COP of the system (Fig. 9).

Fig. 10 provides the modeling results of the mass ratio between MH and reactor in terms of system performance by fixing current density. As the mass ratio Rm increases, the cooling power increases. However, the parasitic loss also increases as more cooling energy is consumed on cooling down the increased MH mass, diminishing return is observed after Rm value of greater than 0.8. After that, the cooling power has no significant improvement. Therefore, there is no point to increase Rm by keep increasing the mass of MH material in the cylindrical reactor.

Table 4 – Physical properties for $LaNi_5$ MH and its reactor.

Parameters	Symbol	Value	Units
Thermal conductivity	k	5	$W \cdot m^{-1} \cdot K^{-1}$
Specific heat	C_{MH}	440	$J \cdot kg^{-1} \cdot K^{-1}$
Density	ρ_{MH}	5000	$kg \cdot m^{-3}$
Reactor inner radius	r_1	0.006	m
Reactor wall thickness	R_{wall}	0.001	m
Reactor height	H_R	0.35	m
Reactor density	ρ_R	7900	$kg \cdot m^{-3}$
Reactor specific heat	C_R	385	$J \cdot kg^{-1} \cdot K^{-1}$

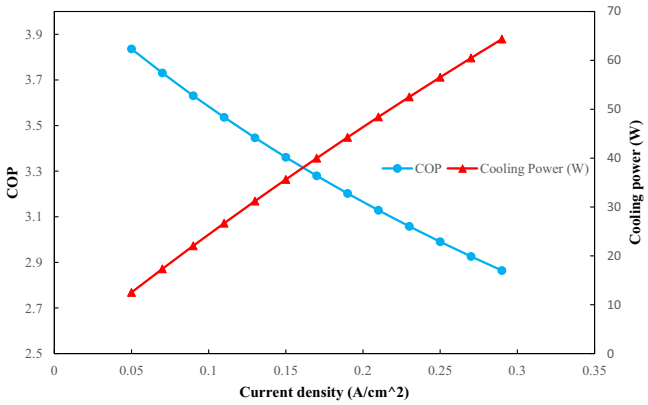

Fig. 8 – Effect of current density on system performance.

The suction and discharge pressure drops on system performance are shown in Figs. 11 and 12. Increase of suction pressure and discharge pressure drop would increase the pressure ratio, and have a marginal effect on the system performance.

Fig. 13 shows the effect of temperature difference between desorption reactor and room temperature on system performance. The temperature difference has a negligible effect on cooling power and suction pressure. However, increase of temperature difference would decrease the system COP significantly, because lowering desorption temperature would lower the EC

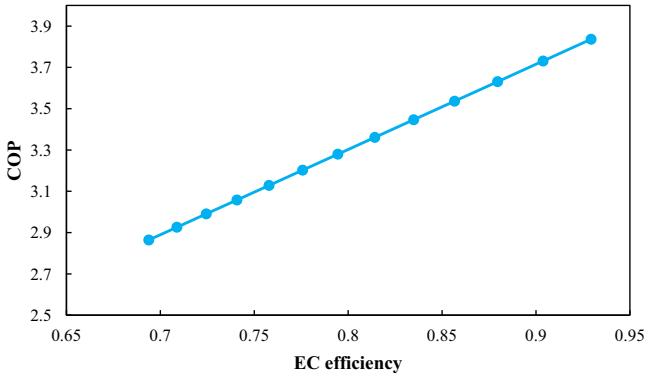

Fig. 9 – Effect of EC efficiency on system performance.

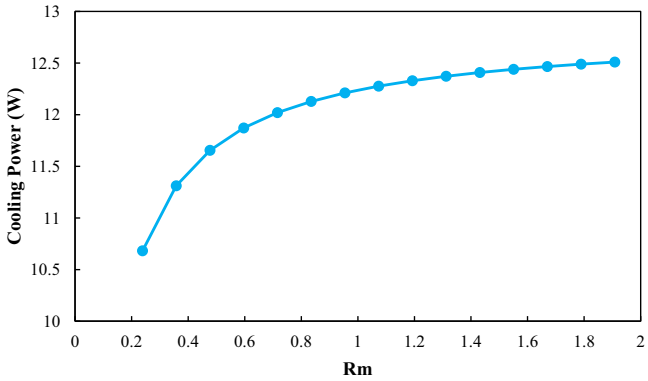

Fig. 10 – Cooling power vs. mass ratio.

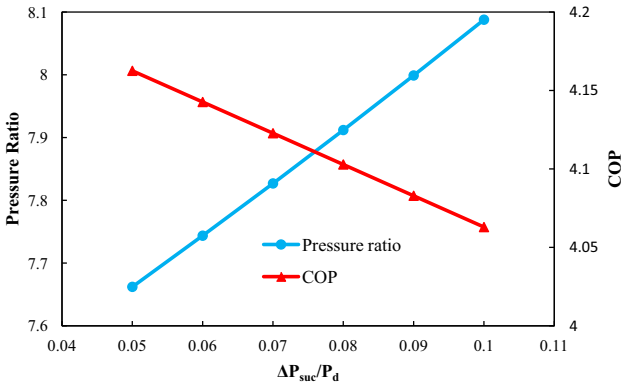

Fig. 11 – Effect of suction pressure drop on system performance.

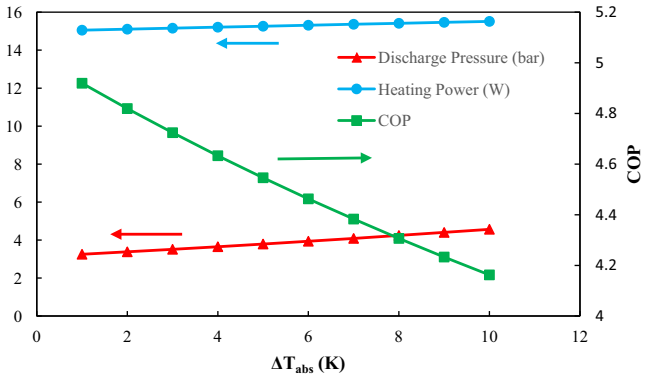

Fig. 14 – Effect of absorption temperature lift on system performance.

suction pressure, which increases the EC power consumption. Fig. 14 shows the effect of temperature difference between the absorption reactor and the heating temperature. Similar to desorption process, the temperature difference has a negligible effect on discharge pressure and heating power. The COP of the system, however, decreases significantly as the temperature difference increases. In order to determine the right suction and discharge pressure drops, the reaction kinetics of MH materials, which generates sufficient desorption and absorption rate for desired performance, has to be considered.

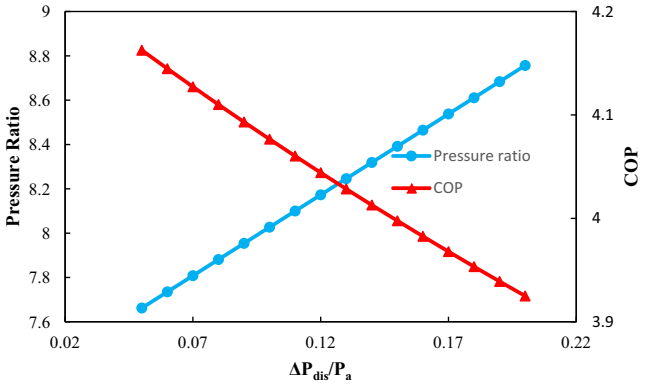

Fig. 12 – Effect of discharge pressure drop on system performance.

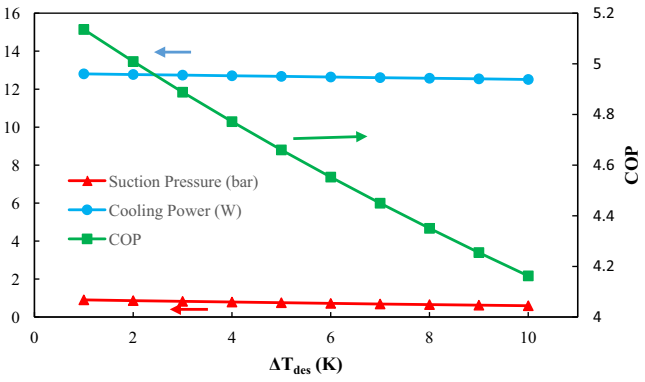

Fig. 13 – Effect of desorption temperature drop on system performance.

Fig. 15 shows the EC stack volume and cooling power in terms of number of cells the stack consists of. For scaling up the system, MEA stacks need to be connected in parallel to increase the hydrogen flow rate. The volume of EC was calculated and compared with the amount of cooling power. It can be determined that a heat pump with 100 W of cooling power and COP of 3.4, at cooling and heating temperatures of 5 °C and 45 °C and current density of 0.15 A·cm^{-2}, requires 70 MEAs to form a 100 × 100 × 700 mm stack. The flow rate control of EC depends on the COP, volume of EC stack and required cooling power because current density generated by external voltage is the driving force of H_2 transport. As shown in Fig. 8, an increase of current density increases the cooling power but reduces the COP. A decrease of current density would increase the number of cell in EC stack in order to achieve the same cooling power as compared to higher current density, therefore, it increases the manufacturing cost. Therefore, there is a balance between the initial cost and the performance, and manufacturers need to take both into consideration for scaling up the system.

The life cycle of EC system is mainly constrained by the EC itself. The EC design is very similar to PEM fuel cell. The life

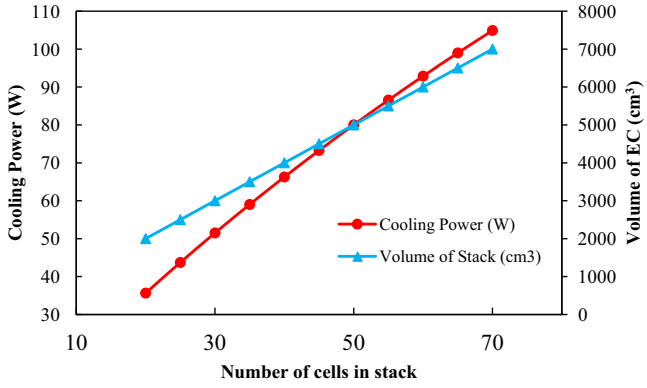

Fig. 15 – Quantitative analysis of EC stack volume and cooling power vs. number of cells in stack.

cycle of PEM fuel cell includes the production of materials and emissions. Pehnt (2001) stated that the production of fuel cell stacks has unneglectable environmental impact. This mainly includes impact caused by the platinum group metal catalyst production and the material and energy consumed for flow field plate production. The emission of SO_2 produced by platinum metal production chain gives major environmental impact. Graphite is the material used for manufacturing the flow field plates. One hundred sixty megajoules of non-renewable energy is consumed to produce 1 kg of graphite, and it is mainly dominated by the electricity of mining and graphitization (Pehnt, 2001).

5. Conclusions

In this study, an EC driven MH heat pump was proposed and studied using thermodynamic models, and its simulation results were discussed. The $LaNi_5$ alloy was selected as a suitable alloy for the MH reactors. The system performance was evaluated based on different parameters. The simulated results show that EC efficiency has a great impact on the system COP. For a small scale heat pump with cooling capacity less than 200 W, the EC operates more efficiently than the mechanical compressor. The EC driven MH heat pump could potentially have a higher COP than the existing MH system. And quantitative analysis shows a heat pump of 100 W cooling power with COP of 3.4 and 5 °C cooling and 45 °C heating temperatures and it requires a $100 \times 100 \times 700$ mm stack. For the future, experimental work needs to be performed to measure the real time performance. Since only the thermodynamic model was presented in this paper, in additional to experiments, transient modeling also needs to be performed for better modeling the system performance.

Acknowledgements

This work is supported by Center for Environmental Energy Engineering, University of Maryland, College Park, MD, USA.

REFERENCES

Barbir, F., 2005. PEM Fuel Cells: Theory and Practice. Elsevier Science, San Diego, Print.

Bedback, S., Gopal, M., 2004. Performance analysis of a compressor driven metal hydride cooling system. Int. J. Hydrogen Energy 30, 1127–1137.

Benziger, J., Bocarsly, A., Cheah, M., Majsztrik, P., Satterfield, B., Zhao, Q., 2011. Mechanical and transport properties of Nafion: effects of temperature and water activity. Struct. Bond. 141, 85–113.

Bouwman, P., 2014. Electrochemical hydrogen compression (EHC) solutions for hydrogen infrastructure. Fuel Cells Bull. 2014, 12–16.

Gardner, C., Ternan, M., 2007. Electrochemical separation of hydrogen from reformate using PEM fuel cell technology. J. Power Sources 171, 835–841.

Goetzler, W., Zogg, R., Young, J., Johnson, C., 2014. Energy Savings Potential and RD&D Opportunities for Non-Vapor-Compression HVAC Technologies. US Department of Energy, Energy Efficiency & Renewable Energy.

Grigoriev, S., Shtatniy, I., Millet, P., Porembsky, V., Fateev, V., 2011. Description and characterization of an electrochemical hydrogen compressor/concentrator based on solid polymer electrolyte technology. Int. J. Hydrogen Energy 36, 4148–4155.

Hirscher, M., 2010. Handbook of Hydrogen Storage: New Materials for Future Energy Storage. Wiley-VCH Verlag GmbH&Co. KGaA, Weinheim.

Hopkins, R., Kim, K., 2010. Hydrogen compression characteristics of a dual stage thermal compressor system utilizing LaNi5 and Ca0.6Mm0.4Ni5 as the working metal hydrides. Int. J. Hydrogen Energy 35, 5693–5702.

Incropera, F., Dewitt, D., 2002. Fundamentals of Heat and Mass Transfer. John Wiley & Sons, Hoboken, NJ, Print.

Kim, K., Feldman, K., Jr., Lloyd, G., Razani, A., 1997. Compressor-driven metal-hydride heat pumps. Appl. Therm. Eng. 17, 551–560.

Lipp, L., 2012. Electrochemical Hydrogen Compressor. DOE Hydrogen Program.

Lipp, L., Patel, P., 2011. Electrochemical Hydrogen Compressor. Department of Energy Hydrogen and fuel Cells Program.

Magnetto, D., Mola, S., Dacosta, D., Golben, M., Rosso, M., 2006. A metal hydride mobile air conditioning system. SAE International, 2006-01-1235.

Mazumdar, S., Gopal, M., Bhattacharyya, S., 2004. Performance of compressor driven metal hydride cooling systems under different operating conditions. International Refrigeration and Air Conditioning Conference, Purdue University, IN.

Mehta, V., Cooper, J., 2002. Review and analysis of PEM fuel cell design and manufacturing. J. Power Sources 114, 32–53.

Moton, J., James, B., Colella, W., 2014. Advances in electrochemical compression of hydrogen. Proceedings of the ASME 2014 12th International Conference on Fuel Cell Science, Engineering and Technology, Boston, MA.

Muthukumar, P., Groll, M., 2010. Metal hydride based heating and cooling systems: a review. Int. J. Hydrogen Energy 35, 3817–3831.

Onda, K., Ichihara, K., Nagahama, M., Minamoto, Y., Araki, T., 2007. Separation and compression characteristics of hydrogen by use of proton exchange membrane. J. Power Sources 164, 1–8.

Park, J., Jang, K., Lee, P., Lee, J., 2001. The operating characteristics of the compressor-driven metal hydride heat pump system. Int. J. Hydrogen Energy 26, 701–706.

Park, J., Han, S., Jang, H., Lee, S., Lee, P., Lee, J., 2002. The development of compressor-driven metal hydride heat pump (CDMHHP) system as an air conditioner. Int. J. Hydrogen Energy 27, 941–944.

Pehnt, M., 2001. Life-cycle assessment of fuel cell stacks. Int. J. Hydrogen Energy 26, 91–101.

Rohland, B., Eberle, K., Strobel, R., Scholta, J., Garche, J., 1998. Electrochemical hydrogen compressor. Electrochim. Acta 43, 3841–3846.

Sandrock, G., 1999. A panoramic overview of hydrogen storage alloys from a gas reaction point of view. J. Alloys Comp. 293–295, 877–888.

Sandrock, G., Bowman, R., Jr., 2003. Gas-based hydride applications: recent progress and future needs. J. Alloys Comp. 356–357, 794–799.

Sedlak, J., Austin, J., LaConti, A., 1981. Hydrogen recovery and purification using the solid polymer electrolyte electrolysis cell. Int. J. Hydrogen Energy 6, 45–51.

Strobel, R., Oszcipok, M., Fasil, M., Rohland, B., Jorissen, L., Garche, J., 2002. The compression of hydrogen in an electrochemical cell based on a PE fuel cell design. J. Power Sources 105, 208–215.

Takeda, H., Kabotomori, T., Ohnishi, K., 2009. Metal hydride air-conditioning, in Energy Carriers and Conversion Systems. In: Ohta, T. (Ed.), Encyclopedia of Life Support Systems (EOLSS), Developed under the Auspices of the UNESCO. EOLSS Publisher, Paris, France. <http://www.eolss.net>.

Wong, T., Girard, F., Vanderhoek, T., 2004. Electrochemical hydrogen compressor, United States patent application publication, 2004/0211679 A1.

Zhong, Y., Glanville, P., 2014. Metal-hydride adsorption systems for space conditioning in commercial and residential buildings. Proceedings of the ASME 2014 International Mechanical Engineering Congress and Exposition, November 14–20, 2014, Montreal, Quebec, Canada.